Solid-State Synthesis and Characterization of Polyaniline/Nano-TiO_2 Composite

Tursun Abdiryim, Aminam Ubul, Ruxangul Jamal, Yuchuan Tian, Tunsagul Awut, Ismayil Nurulla

Key Laboratory of Oil and Gas Fine Chemicals, Ministry of Education and Xinjiang Uygur Autonomous Region, College of Chemistry and Chemical Engineering, Xinjiang University, Urumqi 830046, People's Republic of China

Received 31 October 2011; accepted 21 January 2012
DOI 10.1002/app.36857
Published online in Wiley Online Library (wileyonlinelibrary.com).

ABSTRACT: Polyaniline/nano-TiO_2 composites with the content of nano-TiO_2 varying from 6.2 wt % to 24.1 wt % were prepared by using solid-state synthesis method at room temperature. The structure and morphology of the composites were characterized by the Fourier transform infrared (FTIR) spectra, ultraviolet-visible (UV–vis) absorption spectra, X-ray diffraction (XRD), scanning electron microscopy (SEM), and transmission electron microscopy (TEM). The electrochemical performances of the composites were investigated by galvanostatic charge–discharge measurement, cyclic voltammetry (CV), and electrochemical impedance spectroscopy (EIS). The results from FTIR and UV–vis spectra showed that the composites displayed higher oxidation and doping degree than pure PANI. The XRD and morphological studies revealed that the inclusion of nano-TiO_2 particles hampered the crystallization of PANI chains in composites, and the composites exhibited mixed particles from free PANI particles and the nano-TiO_2 entrapped PANI particles. The galvanostatic charge–discharge measurements indicated that the PANI/nano-TiO_2 composites had higher specific capacitances than PANI. The composite with 6.2 wt % TiO_2 had the highest specific capacitance among the composites. The further electrochemical tests on the composite electrode with 6.2 wt % TiO_2 showed that the composite displayed an ideal capacitive behavior and good rate ability. © 2012 Wiley Periodicals, Inc. J Appl Polym Sci 000: 000–000, 2012

Key words: polymers; composite materials; solid-state synthesis; electrochemical properties

INTRODUCTION

Recently, a great attention has been focused on studying the synthesis and electrochemical properties of electrically conducting polymers, which represent promising electrode materials for the applications of supercapacitors due to their high specific capacitance.[1-5] Among conducting polymers, polyaniline (PANI) has been studied extensively as one of the most promising class of active materials for its applications in electrochromic displays, electrocatalysis, rechargeable batteries, and sensors.[6] Recently, many nanocomposites consisting of PANI with various inorganic nanomaterials have been investigated more and more because their properties are quite different from PANI and corresponding inorganic nanoparticles owing to interfacial interactions between PANI and inorganic nanoparticles. One of the most prevalent type of these composites is composed of materials containing PANI and nano-TiO_2, which have potential applications in supercapacitors,[7] solar sells,[8] microwave absorption,[9] photoelectrochemical devices,[10,11] photocatalysis,[12,13] and corrosion resistant coatings.[14,15]

At the present time, many reports have been published on the preparation of PANI/nano-TiO_2 composites, including chemical oxidative polymerization,[12-17] electrochemical polymerization,[18] ultrasonic irradiation,[19] sol-gel methods,[20] physical mixing,[21] and so on. However, there is no information concerning the fabrication of PANI/nano-TiO_2 composite by solid-state synthesis method and application as supercapacitor. The previous studies showed that the solid-state synthesis method can be used for preparation of polyaniline/nanoparticles composites, but these composites were just the mechanonochemical mixing of nanoparticles and polyaniline prepared without presence of nanoparticles.[22,23] Furthermore, in this method, polyaniline should be prepared before the mechanochemical mixing and it is not the *in situ* polymerization of aniline with the presence of nanoparticles.

As an extension of the traditional synthesis method, solid-state synthesis method has many advantages: reduced pollution, low costs, and

Correspondence to: T. Abdiryim (tursunabdir@sina.com.cn).

Contract grant sponsor: National Natural Science Foundation of China; contract grant number: 20964004 and 21064007.

Contract grant sponsor: Opening Project of Xinjiang Laboratory of Petroleum and Gas Fine Chemicals; contract grant number: XJDX0908-2009-03.

simplicity in process and handling. Now, it is widely used for synthesizing the polyaniline type conducting polymers.[24,25] In solid-state synthesis method, the reaction happens on the surface of solid-sate reactant mainly,[25] and by the milling process reacting solids are contacted together to react with each other. Therefore, interdiffusion rate of the reactants is significantly slower than that of traditional solution method. This means by carefully controlling the experimental conditions to adjust the nucleation and growth of the polymer, solid-state polymerization method could be used to fabricate the nanostructured polymer/inorganic nanoparticles composites.

In this article, we developed a novel solid-state synthesis method for preparation of PANI/nano-TiO_2 composites, and the content of nano-TiO_2 in the composites varied from 6.2 wt % to 24.1 wt %. The correlation between the structures and properties of the PANI/nano-TiO_2 composites were deeply discussed based on the results from FTIR, UV–vis, XRD, SEM, TEM, and CV. Moreover, the potential application of solid-state synthesized PANI/nano-TiO_2 composite as supercapacitor was evaluated by galvanostatic charge–discharge and EIS measurements.

EXPERIMENTAL

Materials

Aniline and ammonium peroxydisulfate ($(NH_4)_2S_2O_8$, APS) of analytical-reagent grade were obtained from Xi'an Chemical Reagent Company (China), *p*-toluenesulphonic acid was obtained from Acros Organics. Nano-TiO_2 (anatase, hydrophilic) with an average size of 40 nm (Shanghai Aladdin Reagent Company, China) was used as received. Aniline was purified by distillation under reduced pressure. All other chemicals and solvents were used as received without further purification.

Preparation of PANI/nano-TiO_2 composites

A typical solid-state synthesis of PANI/nano-TiO_2 composites procedure was as followed: 50 mg nano-TiO_2 and 0.96 g (0.01 mol) aniline were ultrasonicated for 30 min to facilitate TiO_2 to disperse into the aniline monomer, then 1.9 g *p*-TSA was added in this mixture, and then they were put in the mortar. After grinding about 5 min later, the mixture became white paste, 2.2 g APS was added by further grinding for 30 min until the color of solid changed to black green. From these reactions we get pure PANI and PANI/nano-TiO_2 with compositions as given in Table I. The product was washed with ethanol and distilled water, respectively, until the filtrate was colorless, and then the powder dried under vacuum at 60°C for 48 h.

TABLE I
Synthesis of PANI/Nano-TiO_2 Composites with Different Composition

Samples	Aniline wt (g)	TiO_2 wt (g)	Composite yield (g)	TiO_2 in product (wt %)
PANI	0.96	0.0	0.73	0
PT-5	0.96	0.05	0.81	6.2
PT-10	0.96	0.10	0.78	12.8
PT-15	0.96	0.15	0.85	17.6
PT-20	0.96	0.20	0.83	24.1

Structure characterization

The Fourier transform infrared (FTIR) spectra of the composites were obtained by using a BRUKERQEUINOX-55 Fourier transform infrared spectrometer (Billerica, MA) (frequency range 4000–500 cm^{-1}). UV–vis spectra of the samples were recorded on a Shimadzu UV-2450 spectrophotometer. The X-ray diffraction (XRD) studies were performed on a D/Max 2400 X-ray diffractometer by using Cu-Kα radiation source ($\lambda = 0.15418$ nm), the scan range (2θ) was 5° to 60°. Scanning electron microscopy (SEM) measurements were observed on a Leo1430VP microscope. Transmission electron microscopy (TEM) experiments were carried out in a Hitachi 2600 electron microscope. The samples for TEM measurements were prepared by placing a few drops of PANI/nano-TiO_2 ethanol suspension on copper supports.

Electrochemical tests

The electrodes were prepared by mixing 85 wt % active materials (3 mg), 10 wt % carbon black and 5 wt % polytetrafluoroethylene (PTFE) to form slurry. The slurry was pressed on a graphite current collector (area: 1 cm^2), then dried at 60°C for 24 h. The electrochemical behaviors of the composite electrodes were evaluated by cyclic voltammetry (CV), galvanostatic charge–discharge, and electrochemical impedance spectroscopy (EIS) techniques. All electrochemical experiments were carried out in a three-electrode glass cell, a platinum counter electrode, and a standard calomel reference electrode (SCE). CV and galvanostatic charge–discharge tests were performed in the potential window ranged from −0.2 to 0.8 V and conducted at different scan rates and different current densities using CHI660C electrochemical working station. EIS measurements were performed at open-circuit potential by using Zennium40084. Data were collected in the frequency range of 0.1 Hz to100 KHz. The electrolytes were 1*M* H_2SO_4 and 1*M* KCI solution in all the electrochemical tests.

RESULTS AND DISCUSSION

FTIR and UV–vis spectroscopy studies

Figure 1 shows the FTIR spectra of PANI/nano-TiO_2 composites and PANI prepared by solid-state synthesis method. For comparison, the spectrum of nano-TiO_2 is also shown in Figure 1. As can be seen in Figure 1, the FTIR spectra of composites are identical to that of PANI, and there is no characteristic peaks corresponding to the nano-TiO_2 in composites, indicating the nano-TiO_2 is enwrapped by the PANI.[26] The main characteristic bands of PANI appear in the spectra of composites as follows: the band at $\sim$ 3220 cm^{-1} is attributable to N—H stretching vibration; the band at $\sim$ 2921 cm^{-1} can be assigned to the stretching vibration methyl (—CH_3) group in *p*-TSA; the two bands appearing at $\sim$ 1579 cm^{-1} and $\sim$ 1496 cm^{-1} are associated to the stretching vibration of quinoid and benzenoid ring, respectively. The band at $\sim$ 1303 cm^{-1} can be assigned to the C—N mode, while the band at $\sim$ 1145cm^{-1} is the characteristic bands of stretching vibration of quinoid, the bands appearing at $\sim$ 814 cm^{-1} are attributed to an aromatic C—H out-of-plane bending vibration.[16,27] Even though the main bands are similar to those in pure PANI, several discrepancies occur between pure PANI and composites. Comparing the band positions and intensities, it is obvious that the bands shifted slightly from their corresponding position in pure PANI. And the intensity ratio of quinoid to benzenoid units also changes. It can be calculated from the spectra that the value of intensity ratio of quinoid to benzenoid ring modes ($I_{\sim\ 1572\text{-}1578}/I_{\sim\ 1489\text{-}1493}$, where I is absorption intensity) are 0.93, 0.94, 0.92, and 0.97 for the composites,

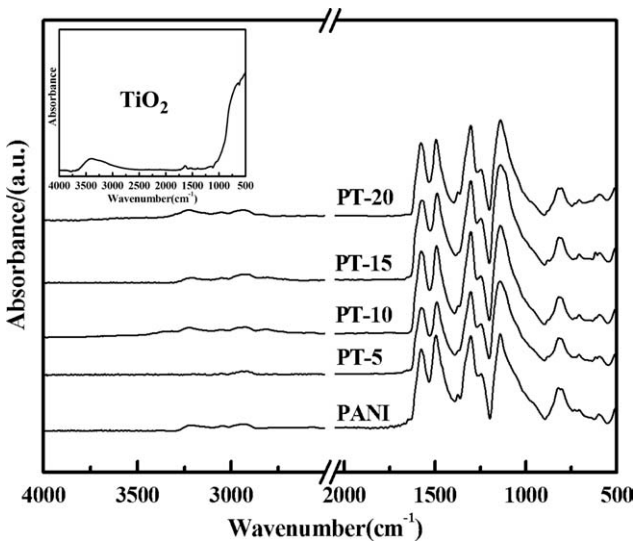

Figure 1 FTIR spectra of PANI, nano-TiO_2 and PANI/nano-TiO_2 composites with content of TiO_2 varying from 6.2 wt % to 24.1 wt %.

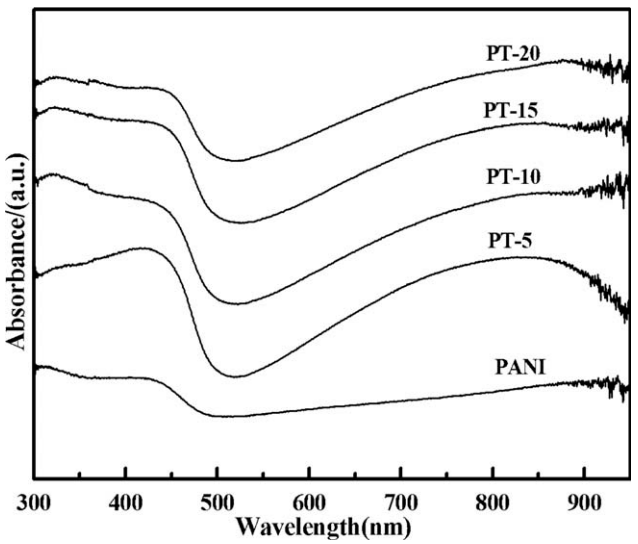

Figure 2 UV–vis spectra of PANI and PANI/nano-TiO_2 composites with content of TiO_2 varying from 6.2 wt % to 24.1 wt %.

respectively, while it is 0.85 for PANI. This suggests that the oxidation degree of composites is higher than PANI. It should be noted here that the presence of nano-TiO_2 content in solid-state reaction will cause the separation of oxidant from the monomer, which in turn facilitates the formation of reduction state of polymer during the oxidative polymerization. This means the oxidation degree of composites should be lower than PANI, which is not so. Therefore, it can be asserted that the nano-TiO_2 has some effects on the oxidation degree of PANI in composites. It is known from the literature that when TiO_2 is excited by the photons of higher than the band gap, electron-hole pairs are generated which in turn react with hydroxyl ion producing reactive radicals of $^{\bullet}O_2^-$ and $HO^{\bullet}$, and these radicals are extremely strong oxidants.[12] In our case, the solid-state polymerization takes place under the visible light, indicating the possibility of formation of these radicals in reaction system. Thus, we can conclude that with the effects of these radicals, the PANI/nano-TiO_2 composites may display higher oxidation degree than PANI.

Figure 2 shows the UV–vis absorption spectra of PANI/nano-TiO_2 composites and PANI in *m*-cresol solution. The PANI/nano-TiO_2 composites and PANI show three characteristic absorption peaks (Table II). The absorption peaks at $\sim$ 316 to 336 nm can be ascribed to π–π^* transition of the benzenoid rings, whereas the peaks at $\sim$ 416 to 428 nm and $\sim$ 836 to 863nm can be attributed to polaron–π^* transition and π–polaron transition, respectively.[24-28] The peak at $\sim$ 316 to 336 nm can also be attributed to the leucoe-meraldine (fully reduced form) of PANI [Fig. 3(a)], and the peak at $\sim$ 836 to 863 nm can be

TABLE II
The Assignments of UV–Vis Absorption Peaks of PANI and PANI/Nano-TiO_2 Composites

Samples	Wave length of absorption peak: π–π* transition (nm)	Polaron–π* transition (nm)	π–polaron transition (nm)	$A_{836–863}/A_{316–336}$
PANI	316	417	863	0.88
PT-5	336	417	836	1.03
PT-10	332	416	845	0.94
PT-15	324	420	844	0.95
PT-20	324	428	863	1.06

explained as the emeraldine salt phases of the PANI [Fig. 3(d)], while the peak at ~ 416 to 428 nm is due to the protonated form of PANI.[28] When comparing the absorption spectra, one can see that the peak positions and intensities of the composites are different from pure PANI, implying some interactions between PANI and nano-TiO_2.[19] According to the previous reports,[17,29] the interactions between PANI and nano-TiO_2 are resulted from following reason: (1) TiO_2 has the tendency to form a coordination compound with nitrogen atoms in PANI;(2) the hydrogen bonding between PANI and nano-TiO_2.

Based on the previous reports, the extent of doping can roughly be estimated from the absorption spectra of PANI, in which the ratio of absorbance at 836 to 863 nm and 316 to 336 nm indicated the doping level of PANI.[24] As shown in Table I, the intensity ratio ($A_{836–863}/A_{316–336}$) of the composites is higher than PANI, suggesting a higher doping level of the composites than PANI. This is quite in accordance with the results of FTIR spectra. The result of FTIR spectra shows that the oxidation degree of composites is higher than PANI, indicating a bigger portion of the quinoid units in composites than in PANI. Consequently, the bigger portion of the quinoid units enhances the doping level of composites.

XRD analysis

Figure 4 shows the X-ray diffraction (XRD) patterns of PANI/nano-TiO_2 composites, PANI, and nano-TiO_2. As shown in Figure 4, the PANI has some degree of crystallinity, and its diffraction peaks locates at about $2\theta = 9.6°$, 19.4°, 25°. The peak at lowest angle ($2\theta = 9.6°$) is considered to be the distance between two stacks in the two-dimensional stacking arrangement of polymer chains with intervening dopant ions between stacks, and the peak centered at $2\theta = 19.4°$ may be ascribed to periodicity parallel to the polymer chain,[30,31] while the peaks at $2\theta = 25°$ may be caused by the periodicity perpendicular to the polymer chain. The peak at $2\theta = 25°$ also represents the characteristic distance between the ring planes of benzene rings in adjacent chains or the close-contact interchain distance.[30,31] From the XRD patterns of the composites, it can be seen that the nano-TiO_2 (major peaks: 25°, 37.8°, 48°, 53.8°, and 55°) is also present in these composites. The diffraction patterns of the composites are similar to that of nano-TiO_2. This result means that the presence of PANI has no influence on crystallization performance of nano-TiO_2.[19] Furthermore, as the nano-TiO_2 content in the composites increases, the diffraction peak of PANI at $2\theta = \sim 25°$ becomes sharper and more intense, revealing that the composites are more crystalline than PANI.

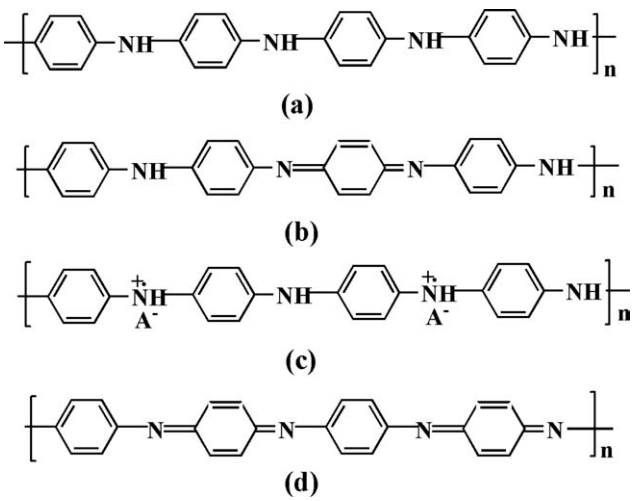

Figure 3 Four different redox forms of PANI:(a) leucoemeraldine base (fully reduced form), (b) emeraldine base (half-oxidized form), (c) conducting emeraldine salt (half-oxidized and protonated form), and (d) pernigraniline base (fully oxidized form).

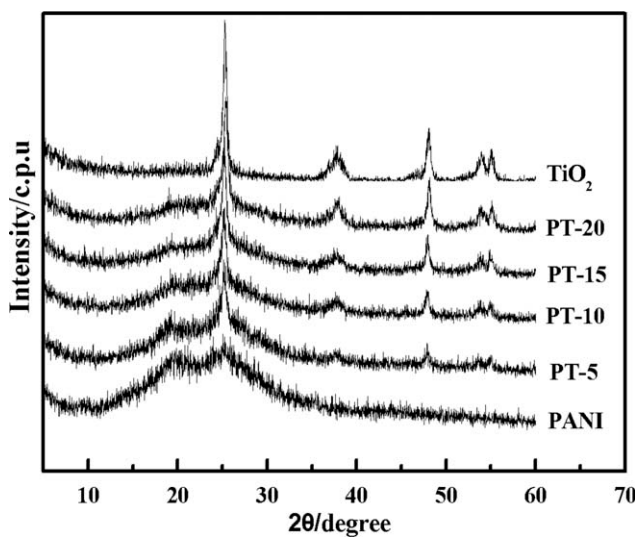

Figure 4 XRD patterns of PANI, nano-TiO_2, and PANI/nano-TiO_2 composites with content of TiO_2 varying from 6.2 wt % to 24.1 wt %.

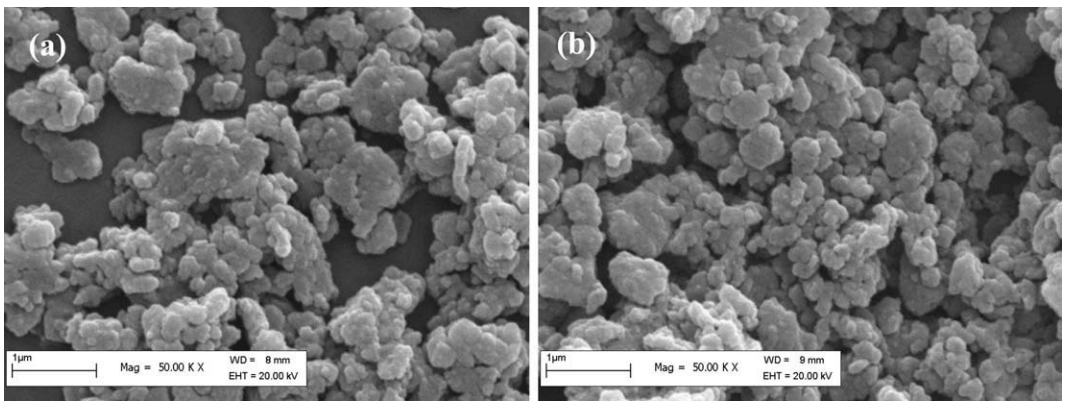

Figure 5 SEM images of the PANI/nano-TiO_2 composites with (a) 6.2 wt %TiO_2 and (b) 17.6 wt % TiO_2.

Morphology

Figure 5 shows the SEM images of the PANI/nano-TiO_2 composites with 6.2 wt % and 17.6 wt % TiO_2, respectively. As can be seen from the Figure 5, the particles of the PANI/nano-TiO_2 composites are highly aggregated, but the separate particles show that the particle size is smaller than 200 nm. Figure 6 reveals the TEM images of the nano-TiO_2, PANI, and PANI/nano-TiO_2 composites (6.2 wt % TiO_2 and 17.6 wt % TiO_2). As shown in Figure 6(a), the nano-TiO_2 are "rice-like" nanoparticles with an average size of 40nm. In Figure 6 (b), it shows the PANI particles display the spherical shape with smaller size than 100 nm. After the formation of the composites [Fig. 6(c,d)], the nano-TiO_2 particles (dark-shaded nanoparticles) are found to be entrapped into PANI (light shaded) matrix. This means that the nano-TiO_2 particles are not simply mixed up or blended with the polymer, which is similar to the earlier report about the PANI/nano-TiO_2 composites synthesized by the inverted emulsion polymerization method.[32] It is obvious from Figure 6(c,d), the dark-shaded nanoparticles (nano-TiO_2) in the composite with 17.6 wt % TiO_2 are more than the composite with 6.2 wt % TiO_2. Furthermore, the free PANI particles can be observed in composite with 6.2 wt % TiO_2, and size of the composite particles are smaller than the composite with 17.6 wt % TiO_2.

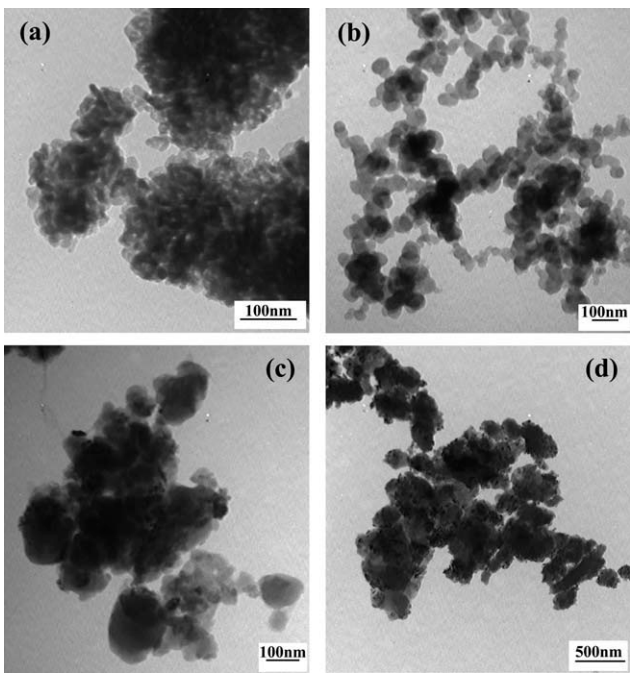

Figure 6 TEM images of the nano-TiO_2 (a), PANI (b), PANI/nano-TiO_2 composites with (c) 6.2 wt % TiO_2, and (d) 17.6 wt % TiO_2.

Electrochemical properties

Figure 7 shows the galvanostatic charge–discharge curves of PANI and PANI/nano-TiO_2 composites at a current density of 3 mA cm^{-2} in three-electrode

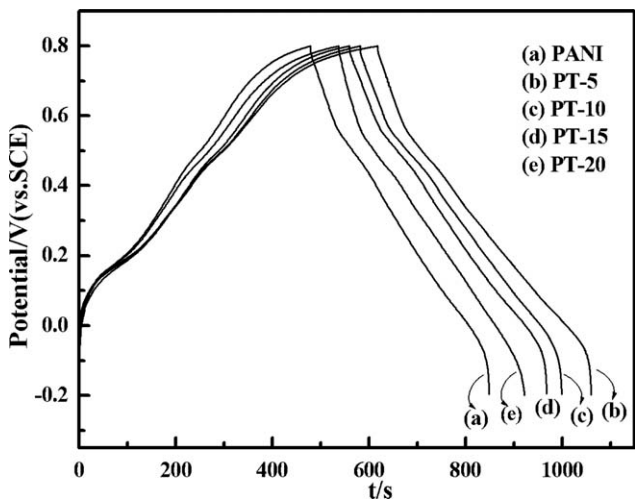

Figure 7 Galvanostatic charge–discharge curves of PANI and PANI/nano-TiO_2 composite electrodes at current density of 3 mA cm^{-2} in 1*M* H_2SO_4 electrolyte. Mass of the active material: 3 mg

system between −0.2 and 0.8 V, and the supporting electrolyte is 1*M* H_2SO_4. The specific capacitance (SC) of the electrode material can be calculated by means of SC = $(I \times \Delta t)/(\Delta V \times m)$,[33] where I is charge–discharge current, Δt is the discharge time, ΔV is the electrochemical window (1V), and m is the mass of active materials within the electrode (3 mg). The specific capacitances of PANI and PANI/nano-TiO_2 composites calculated from Figure 7 are 370 fg^{-1} (PANI), 442 fg^{-1}(6.2 wt % TiO_2), 421 fg^{-1}(12.8 wt % TiO_2), 410 fg^{-1}(17.6 wt % TiO_2), and 385 fg^{-1}(24.1 wt % TiO_2), respectively. In comparison with the pure PANI, the composites show a higher SC, and the respective SC is higher than oxidative polymerized PANI/nano-TiO_2 composite reported by Bian et al.[7] This enhanced SC may be resulted from the contribution of nano-TiO_2, which is very advantageous to reduce the electrochemical degradation of PANI and improve its capacitance as electrode material. [7] Furthermore, it is concluded from the FTIR spectra and UV–vis absorption spectra that the composites have higher oxidation degree and doping level than PANI, which in turn enhances the electrochemical activities of these composite electrodes. In addition, nanosized particles may provide a large surface area and allow excellent electrolyte access in three dimensions. However, it should be noted that the conductivity of pure nano-TiO_2 is very low ($\sim 10^{-6}$ S cm^{-1}),[34] and its corporation with PANI should bring some decrease in electrochemical activity of composites. This prediction is further proved by the changes in SC of composites, which implies that SC decreases gradually with the increase of nano-TiO_2 content. Therefore, the lowest SC value of the composite with 24.1 wt % TiO_2, which has the high oxidation degree and doping level, should be resulted from the largest amount of nano-TiO_2 content, causing a decrease in electrochemical activity of the composite.

To further investigate the electrochemical capacitance of the PANI/nano-TiO_2 composite, a series of electrochemical tests such as galvanostatic charge–discharge measurement, cyclic voltammetry (CV), and electrochemical impedance spectroscopy (EIS) were performed on PT-5 (composite with the content of 6.2 wt % TiO_2). Figure 8 shows galvanostatic charge–discharge tests of PT-5 between −0.2 and 0.8 V at various current densities of 10, 15, 20, 25 mA cm^{-2} in three-electrode system. The supporting electrolytes are 1*M* H_2SO_4 and 1*M* KCl, respectively.

As shown in Figure 8, the highest SC of the composite were 490 fg^{-1} in 1*M* H_2SO_4 and 415 F/g in 1*M* KCl at 10 mA/cm^2, respectively. All the curves both in 1*M* H_2SO_4 [Fig. 8(a)] and 1*M* KCl [Fig. 8(b)] are not ideal straight line, indicating the process of a faradic reaction. Moreover, there is an initial drop in potential caused by internal resistance. The charge–discharge curves [Fig. 8(a)] in 1*M* H_2SO_4 exhibit mirror-like images, suggesting a reversible oxidation process and better electrochemical capacitance performance in acidic electrolyte compared with that in neutral electrolyte. Comparing with the SC (421 fg^{-1}) at 3 mA cm^{-2} (Fig. 7), the SC at 10 mA cm^{-2} [Fig. 8(a)] displayed higher value (490 fg^{-1}) in 1*M* H_2SO_4. This is similar to the earlier report, in which that the discharge capacitance of the PANI nanowire arrayed electrodes synthesized by means of anodic deposition technique increases with increasing of charge–discharge current densities.[35]

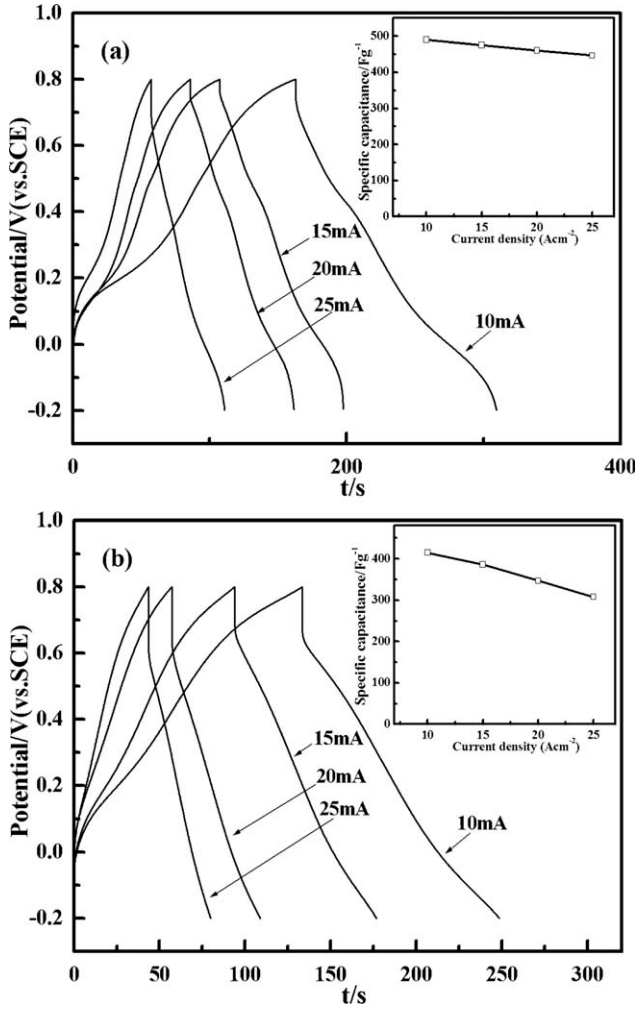

Figure 8 Galvanostatic charge–discharge curves of PANI/nano-TiO_2 composite with 6.2 wt % TiO_2 electrode at various current densities in (a) 1*M* H_2SO_4 electrolyte and (b) 1*M* KCl electrolyte. Mass of the active material: 3 mg.

According to the previous report, this increase of the SC for the composite electrode may be attributed to the existence of various forms of pores and pore diameters in the electrode resulted from the different nanosized structure, and it seems that some pores with small diameter can be invaded by ions from the electrolyte with high charging current.[36] It is

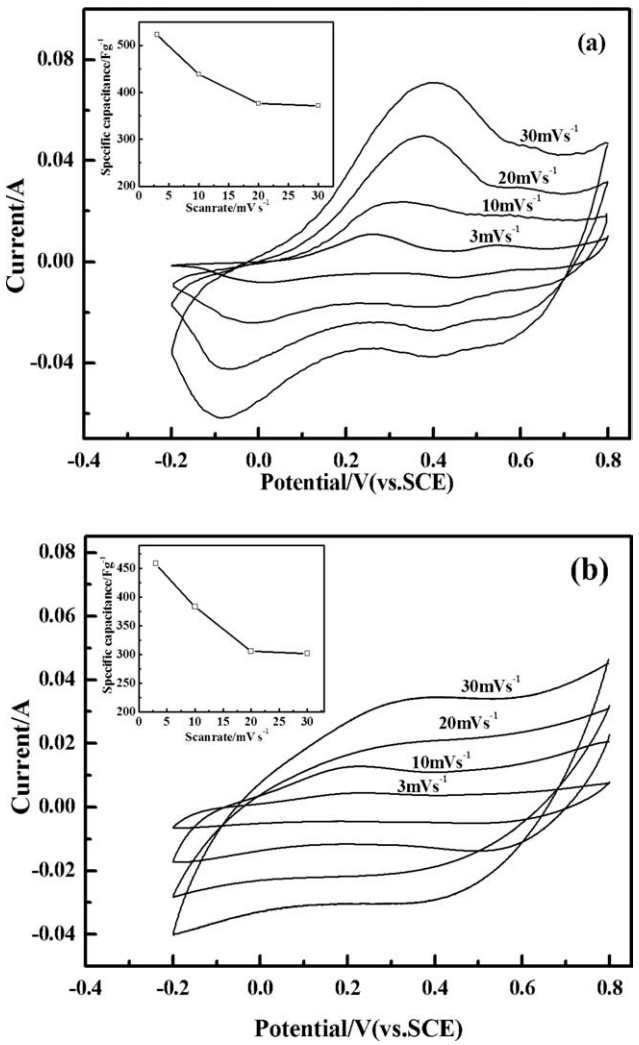

Figure 9 CV curves of PANI/nano-TiO_2 composite with 6.2 wt % TiO_2 electrode at various scan rates in (a) 1*M* H_2SO_4 electrolyte and (b)1*M* KCl electrolyte. Mass of the active material: 3 mg.

noted in Figure 8, the SC gradually decreases after the increase of current density from 10 mA cm^{-2} to 25 mA cm^{-2}, and it is in accordance with the common believe that the SC decreases with the increasing of current density.[7] In general, SC decreases with the growth of current density, the reason is that the electrolyte ion cannot penetrate well into the inner of active materials due to slow diffusion at large current density. However, in this case, the corresponding capacitance retention ratio still reach circa 90% with growth of current densities from 10 to 25 mA cm^{-2}, indicating this composite electrode material can be maintained under very high power operations, which is significant for the electrode material of supercapacitor to afford the higher specific capacitance.[35]

Figure 9 shows the CV curves of PT-5 (composite with the content of 6.2 wt % TiO_2) electrode measured from -0.2 to 0.8 V at different scan rates in three-electrode system. The supporting electrolytes are 1*M* H_2SO_4 [Fig. 9(a)] and 1*M* KCl [Fig. 9(b)], respectively. A comparison indicates that the all curves displayed two pairs of oxidation and reduction peaks in 1*M* H_2SO_4, and no obvious peak is found on the positive and negative sweeps in 1*M* KCl. In the positive sweep, the first redox peak [Fig. 9(a)], $\sim 0.3/\sim 0.01$ V) is well known as the formation of radical cations (polaronic emeraldine) and the second redox couple [Fig. 9(a)], $\sim 0.77/\sim 0.67$V) is the formation of diradical dications (represented by the resonance structures: bipolaronic pernigraniline and protonated quinonediimine) through the oxidation of PANI salts.[37,38] Between this two main pairs of redox peaks, a relatively low intensity peaks [Fig. 9(a)], $\sim 0.6/\sim 0.4$V) have been associated to the degradation of PANI salts.[39] When the scan rate increased from 3 to 30 mV s^{-1}, the peak current rapidly increases, indicating a good rate ability of the composite electrode both in acidic and neutral solution.

Previous studies show that the specific capacitance (SC) of the electrode can also be estimated from the CV curves, and the formula is $C = \int_{E_1}^{E_2} i(E)dE/2vm(E_2 - E_1))$,[40] where C is the specific capacitance (SC) of individual sample. E_1, E_2 are the cutoff potentials in cyclic voltammetry. $i(E)$ is the instantaneous current. $\int_{E_1}^{E_2} i(E)dE$ is the total voltammetric charge obtained by integration of positive and negative sweep in cyclic voltammograms. $(E_2 - E_1)$ is the potential window width, and m is the mass of the individual sample. The variation in the SC of the electrodes as a function of the scan rates is plotted in the inserted image. The SC of the composite calculated from Figure 9(a) are 523, 439, 376, and 372 fg^{-1}, while the corresponding values from Figure 9(b) are 458, 383, 306, and 302 fg^{-1} at the various scan rates. Herein, the SC of the composite electrode decreases along with the increase of scan rate, and the decreasing speed of SC with increasing scan rate is also larger in 1*M* KCl solution than in 1*M* H_2SO_4, which is consistent with the results of galvanostatic charge–discharge tests. However, it should be noted that the SC calculated form CV are different from those derived from galvanostatic charge–discharge test, which is mainly due to the different testing systems applied.

Electrochemical impedance spectroscopy (EIS) has been widely used to study the redox processes of electrically conducting polymers. The EIS measurements of PT-5 (composite with the content of 6.2 wt % TiO_2) electrode at the open-circuit potential with ac-voltage amplitude of 5 mV over the frequency range of 0.1 Hz to 100 KHz are given in Figure 10. As shown in Figure 10, the EIS plots contain two well–separated patterns. First, the high frequency intercept of the semicircle with the real axis can be

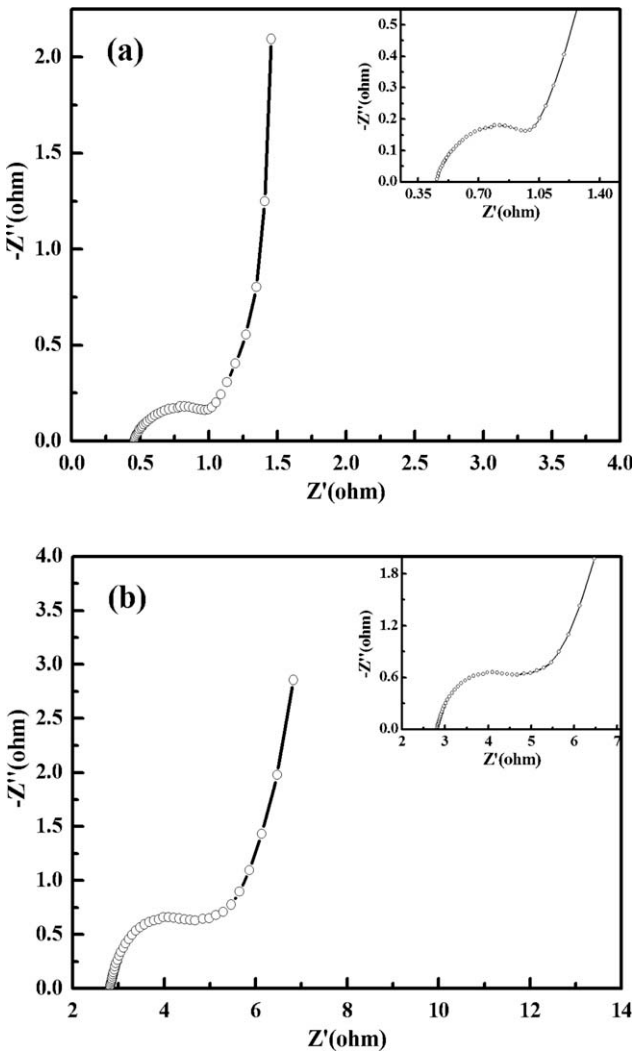

Figure 10 EIS curves of PANI/nano-TiO_2 composite with 6.2 wt % TiO_2 electrode at open-circuit potential with ac-voltage amplitude of 5 mV over the frequency range of 10^{-1} to 10^5 Hz in (a) 1*M* H_2SO_4 electrolyte and (b) 1*M* KCl electrolyte. Mass of the active material: 3 mg.

used to evaluate the value of internal resistance, which included the resistance of the electrolyte solution, the intrinsic resistance of the active material, and the contact resistance at the interface active material/current collector. Its value is approximately 0.46Ω in 1*M* H_2SO_4 and 2.8Ω in 1*M* KCl electrolyte, respectively. The radius of the semicircular in 1*M* H_2SO_4 electrolyte is (0.17) smaller than that in 1*M* KCl electrolyte (0.65). This implies that the charge transfer resistance is smaller in acidic electrolyte. Second, the imaginary impedance at low frequency reveals a slightly tilted vertical line of a limiting diffusion process in two electrolytes, which is characteristic feature of pure capacitive behavior.[41] All these results further manifests that PANI/nano-TiO_2 composites can be used as electrode material for supercapacitors.

CONCLUSION

In this article, a solid-state synthesis method was developed for the preparation of PANI/nano-TiO_2 composites. The results showed that the presence of nano-TiO_2 in solid-state oxidative polymerization process will lead the PANI in composites displaying a higher oxidation and doping degree than the pure PANI. The results also revealed that the composites were not the simple mixture of PANI and nano-TiO_2, and the composites exhibited mixed particles from free PANI particles and the nano-TiO_2 entrapped PANI particles. The electrochemical tests on the PANI/nano-TiO_2 composite electrode with 6.2 wt % TiO_2 showed that the composite displayed an ideal capacitive behavior and good rate ability with high specific capacitance. All electrochemical results also suggest that the solid-state synthesized PANI/nano-TiO_2 composites can be used as electrode material for supercapacitors. More importantly, the solid-state synthesis method might be facile but effective and could be readily used for a large-scale preparation of the PANI/nano-TiO_2 composites, indicating a potential application in fabricating the composites of nano-TiO_2 with PANI.

References

1. Belanger, D.; Ren, X.M.; Davey, J.; Uribe, F.; Gottesfeld, S. J Electrochem Soc 2000, 147, 2923.
2. Jurewicz, K.; Delpeux, S.; Bertagna, V.; Beguin, F.; Frackowiak, E. Chem Phys Lett 2001, 347, 36.
3. Arbizzani, C.; Gallazzi, M.C.; Mastragostino, M.; Rossi, M.; Soavi, F. Electrochem Commun 2001, 3, 16.
4. Prasad, K.R.; Munichandraiah, N. J Electrochem Soc 2002, 149, 1393.
5. Ryu, K.S.; Kim, K.M.; Park, Y.J.; Park, N.G.; Kang, M.G.; Chang, S.H. Solid State Ionics 2002, 152, 861.
6. Novak, P.; Muller, K.; Santhanam, K.S.V.; Haas, O. Chem Rev 1997, 97, 207.
7. Bian, C.Q.; Yu, A.S.; Wu, H.Q. Electrochem Commun 2009, 11, 266.
8. Li, Q.; Wu, J.; Tang, Q.; Lan, Z.; Li, P.; Lin, J.; Fan, L. Electrochem Commun 2008, 10, 1299.
9. Phang, S.W.; Tadokoro, M.; Watanabe, J.; Kuramoto, N. Curr Appl Phys 2008, 8, 391.
10. Su, S.J.; Kuramoto, N. Synth Met 2000, 114, 147.
11. Ilieva, M.; Ivanov, S.; Tsakova, V. J Appl Electrochem 2008, 38, 63.
12. Li, X.Y.; Wang, D.S.; Cheng, G.X.; Luo, Q.Z.; An, J.; Wang, Y.H. Appl Catal B 2008, 81, 267.
13. Zhang, X.Q.; Yan, G.L.; Ding, H.M.; Shan, Y.K. Mater Chem Phys 2007, 102, 249.
14. Sathiyanarayanan, S.; Azim, S.S.; Venkatachari, G. Electrochim Acta 2007, 52, 2068.
15. Radhakrishnan, S.; Siju, C.R.; Mahanta, D.; Patil, S.; Madras, G. Electrochim Acta 2009, 54, 1249.
16. Chuang, F.; Yang, S. Synth Met 2005, 152, 361.
17. Xu, J.C.; Liu, W.M.; Li, H.L. Mater Sci Eng C 2005, 25, 444.
18. Ilieva, M.; Ivanov, S.; Tsakova, V. J Appl Electrochem 2008, 38, 63.
19. Wang, F.; Min, S.X. Chin Chem Lett 2007, 18, 1273.

20. Jang, S.H.; Han, M.G.; Im, S.S. Synth Met 2000, 110, 17.
21. Zhang, H.; Zong, R.L.; Zhao, J.C.; Zhu, Y.F. Environ Sci Technol 2008, 42, 3803.
22. Aleksandrov, I.; Karmilov, A.; Solodovnikov, S. Polym Sci Ser B 2009, 51, 309.
23. Yoshimoto, S.; Ohashi, F.; Ohnishi, Y.; Nonami, T. Synth Met 2004, 145, 265.
24. Tursun, A.; Zhang, X.G.; Ruxangul, J. Mater Chem Phys 2005, 90, 367.
25. Huang, J.; Moore, J.A.; Acquaye, J.H.; Kaner, R.B. Macromolecules 2005, 38, 317.
26. Li, Q.L.; Zhang, C.R.; Li, J.Q. Appl Surf Sci 2010, 257, 944.
27. Nagaraja, M.; Pattar, J.; Shashank, N.; Manjanna, J.; Kamadc, Y.; Rajanna, K.; Mahesh, H.M. Synth Met 2009, 159, 718.
28. MacDiarmid, A.G.; Epstein, A.J. Synth Met 1994, 65, 103.
29. Li, X.W.; Wang, G.C.; Li, X.X.; Lu, D.M. Appl Surf Sci 2004, 229, 395.
30. Pouget, J.P.; Jozefowicz, M.E.; Epstein, A.J.; Tang, X.; MacDiarmid, A.G. Macromolecules 1991, 24, 779.
31. Moon, Y.B.; Cao, Y.; Smith, P.; Heeger, A.J. Poly Commun 1989, 30, 196.
32. Mohammad, R.K.; Hyun, W.L.; In, W.C.; Sung, M.P.; Weontae, O.; Jeong, H.Y. Polym Compos 2010, 31, 83.
33. Ryu, K.S.; Lee, Y.; Han, K.S.; Park, Y.J.; Kang, M.G.; Park, N.G.; Chang, S.H. Solid State Ionics 2004, 175, 765.
34. Lia, X.W.; Wang, G.C.; Li, X.X.; Lu. D.M. Appl Surf Sci 2004, 229, 395.
35. Zhao, G.Y.; Li, H.L. Microporous Mesoporous Mater 2008, 110, 590.
36. An, K.H.; Jeon, K.K.; Heo, J.K.; Lim, S.C.; Bae, D.J.; Lee, Y.H. J Electrochem Soc 2002, 149, 1058.
37. Stilwell, D.E.; Park, S.M. J Electrochem Soc 1988, 135, 2254.
38. Yang, C.H.; Wen, T.C. J Appl Electrochem 1994, 24, 166.
39. Doic, L.; Mandic, Z. Electrochim Acta 1995, 40, 1681.
40. Chen, W.; Fan, Z.L.; Gu, L.; Bao, X.H.; Wang, C.L. Chem Commun 2010, 46, 3905.
41. Mi, H.Y.; Zhang, X.G.; Ye, X.G.; Yang, S.D. J Power Sources 2008, 176, 403.